ACADÉMIE
DES SCIENCES
INSTITUT DE FRANCE

Comptes Rendus
Chimie

Fatima Zahra Tabane, Rachid Fakhreddine, Hajar Bellefqih, Aziz Zaroual, Saida Krimi and Abderrahim Aatiq

Study and characterization of iron orthophosphate $BaSb_{0.5}Fe_{0.5}(PO_4)_2$

Volume 29 (2026), p. 207-216

https://doi.org/10.5802/crchim.439

The Comptes Rendus. Chimie *are a member of the Mersenne Center for open scientific publishing*
www.centre-mersenne.org — e-ISSN : 1878-1543

ACADÉMIE DES SCIENCES
INSTITUT DE FRANCE

Comptes Rendus. Chimie
2026, Vol. 29, p. 207-216
https://doi.org/10.5802/crchim.439

Research article

Study and characterization of iron orthophosphate $BaSb_{0.5}Fe_{0.5}(PO_4)_2$

Fatima Zahra Tabane [*,a], Rachid Fakhreddine [a], Hajar Bellefqih [b], Aziz Zaroual [c], Saida Krimi [a] and Abderrahim Aatiq [d]

[a] Laboratory of Génie des Matériaux, des Procédés et de l'Environnement (GeMaPE), Faculty of Sciences Ain Chock, Hassan II University, Casablanca, Morocco

[b] Ecole Nationale Supérieure des Mines de Saint Etienne, CNRS UMR, EVS, 5600, F42023 Saint Etienne, France

[c] Laboratory of Materials Nanotechnology and Environment, Faculty of Sciences Rabat, Mohamed V University, Rabat, Morocco

[d] Faculty of Sciences Ben Sick, University Hassan II of Casablanca, Morocco

E-mail: tabanefatimazahra@gmail.com (F. Z. Tabane)

Abstract. In this paper, we report the synthesis, structural, vibrational, and optical characterization of the $BaSb_{0.5}Fe_{0.5}(PO_4)_2$ compound, prepared via the conventional solid-state reaction method. X-ray powder diffraction analysis, followed by Rietveld refinement, revealed that the material crystallizes in the monoclinic system with the $C2/m$ space group and $Z = 2$, consistent with a yavapaiite-type structure. Scanning electron microscopy was employed to examine the microstructure and confirm elemental homogeneity. Raman and infrared spectroscopy were used to investigate the internal modes of the phosphate units, providing evidence for well-defined PO_4^{3-} tetrahedra and confirming the integrity of the crystal framework. UV–visible spectroscopy measurements indicated both direct and indirect optical band gap energies of 2.96 and 3.28 eV, respectively, suggesting that $BaSb_{0.5}Fe_{0.5}(PO_4)_2$ behaves as a semiconducting material. The combination of a well-ordered crystal structure, vibrational stability, and semiconducting properties highlights the potential of this phosphate-based compound for applications in optoelectronic devices and functional materials.

Keywords. Iron orthophosphate, Solid-state reaction, Scanning electron microscopy, Optoelectronics.

Note. Submitted by invitation as part of the 13th edition of the Moroccan Meetings on Solid State Chemistry (REMCES-13).

Manuscript received 3 June 2025, revised 3 December 2025, accepted 17 December 2025.

1. Introduction

In recent years, phosphate-based compounds have garnered considerable attention within the scientific community owing to their intrinsic structural diversity and the breadth of their potential technological applications. The fundamental building units of these materials, PO_4 tetrahedra, enable the construction of a wide array of crystalline architectures, allowing the systematic modulation of physical and chemical properties through compositional and structural variation. This versatility has rendered phosphate frameworks especially attractive for use in fields such as energy storage, catalysis, ion exchange, and solid-state ion conduction.

Within this broad class of materials, transition-metal phosphates have emerged as particularly promising candidates. Their utility stems from a unique combination of chemical robustness, redox

* Corresponding author

flexibility, and tunable framework geometries. Several structural families have been extensively studied for their performance in various technological domains. Among them, phosphates of the NASICON (sodium super ionic conductor) type have drawn significant interest due to their three-dimensional open-framework structures and exceptional ionic conductivity, which are ideal for lithium- and sodium-ion battery applications [1,2]. Likewise, diphosphates and langbeinite-type phosphates have been explored for their thermal stability and catalytic efficiency in both environmental and industrial processes [3–5]. Monophosphates, which are structurally simpler yet chemically versatile, have shown promise in electrochemical devices and ion transport systems [6–10].

A notable subcategory within monophosphates comprises compounds with general formula $A^{II}M^{IV}(PO_4)_2$, where A^{II} represents a divalent cation (e.g., Ca^{2+}, Sr^{2+}, Ba^{2+}) and M^{IV} denotes a tetravalent cation (e.g., Zr^{4+}, Sn^{4+}, Ti^{4+}). These materials have been the focus of several structural studies aiming to correlate chemical composition with crystallographic arrangement. Two primary structural types have been identified in this family: cheralite-type and yavapaiite-type frameworks. The distinction between these two polymorphs is governed predominantly by the relative sizes of the constituent cations.

Specifically, a high ionic-radius ratio between the A^{II} and M^{IV} cations favors the formation of the yavapaiite-type structure, characterized by an ordered network of cationic polyhedra. This structural order is typically associated with enhanced material stability and predictable ion transport pathways, which are desirable for energy storage and ionic conduction applications. In contrast, systems with a lower radius ratio tend to crystallize in the cheralite-type structure, which exhibits a more disordered arrangement of cations. While such disorder can be detrimental to certain properties such as ionic mobility it may, in some contexts, introduce defect-mediated functionalities that are beneficial in applications like heterogeneous catalysis or proton conduction [10].

These insights into the structure–composition relationships within $A^{II}M^{IV}(PO_4)_2$ compounds offer a rational basis for the design and optimization of phosphate-based materials. By carefully selecting suitable cation pairs, it is possible to direct the formation of targeted structures with tailored properties, thereby advancing the development of high-performance materials for next-generation electrochemical and catalytic technologies.

Recently, diverse compounds $A(M^{V}_{0.5}X^{III}_{0.5})(PO_4)_2$ with M = Sb, Nb; A = Sr, Pb, Ba; and X = Ga, Cr, Fe, Sc, In, Yb, Al have been studied in terms of structural and vibrational properties [11–18]. The barium phases $Ba(X^{III}_{0.5}X'^{V}_{0.5})(PO_4)_2$ crystallized in the monoclinic $C2/m$ space group ($Z = 2$), while other phases such as $A(Sb_{0.5}X^{III}_{0.5})(PO_4)_2$ (A: Pb, Sr; X: Fe, Cr, Ga) [11,13,14] crystallized in the distorted monoclinic yavapaiite structure type, of space group $C2/c$ ($Z = 4$).

Searching UV–visible spectra of novel semiconducting phosphates, this paper investigates microstructural, vibrational properties of the $BaSb_{0.5}Fe_{0.5}(PO_4)_2$ space group ($C2/m, Z = 2$) [11]. In this context, microstructural morphology, Raman and infrared spectra and UV–visible absorption spectra are studied for optical properties of this phosphate.

2. Experimental

2.1. *Synthesis*

The $BaSb_{0.5}Fe_{0.5}(PO_4)_2$ compound was prepared using the conventional high-temperature solid-state process from mixtures of $BaCO_3$, Fe_2O_3, Sb_2O_3, and $NH_4H_2PO_4$ powders in an appropriate stoichiometric ratio. The reagents were transferred to an agate mortar and finely ground into a perfectly homogeneous mixture, which was then heated in air to a final temperature of 930 °C.

2.2. *Characterization techniques*

The X-ray powder diffraction (XRD) pattern of the resulting material was collected at room temperature using a D8 Advance Bruker diffractometer equipped with Cu anticathode (Cu–Kα radiation, $\lambda = 1.5406$ Å) and Lynx Eye detectors. The measurements were performed under Bragg–Brentano geometry at 2θ with 0.0105° steps in the 10°–80° range. Structural refinements were carried out using the FullProf Suite software [19].

Infrared spectra of the compounds were recorded using Bruker's VERTEX 70 FTIR spectrometer in the 1500–400 cm^{-1} range, with the samples prepared as KBr pellets. Raman spectra were recorded on the RENISHAW 1000B spectrometer in the 50–1500 cm^{-1} range.

The microstructural surface features of the samples were examined using scanning electron microscopy (SEM) with a JEOL JSM-IT100 InTouchScope microscope, operated at 15 kV. Prior to imaging, the sample was mounted on aluminum stubs using carbon tape and coated with a thin layer of carbon through metallization to ensure surface conductivity and to avoid charging effects. The observations were made at various magnifications (3000× at 20 μm and 2000× at 30 μm).

3. Results and discussion

3.1. *Structure of $BaSb_{0.5}Fe_{0.5}(PO_4)_2$ phase*

The Rietveld study, performed using the Le Bail profile, revealed that the $BaSb_{0.5}Fe_{0.5}(PO_4)_2$ phase crystallizes in the monoclinic $C2/m$ space group. Accordingly, the initial structural parameters for the Rietveld refinement were adopted from the previously reported $BaSb_{0.5}Ga_{0.5}(PO_4)_2$ phase by Fakhreddine et al. [14], which also belongs to the $C2/m$ space group. The refinement yielded satisfactory reliability indicators, with $R_F = 1.6\%$, $R_B = 2.2\%$, and $\chi^2 = 1.3$. The Rietveld refinement for the $BaSb_{0.5}Fe_{0.5}(PO_4)_2$ compound is illustrated in Figure 1, while the detailed refinement parameters are summarized in Table 1. Table 2 presents the XRD data obtained from the "observed intensities" of the Rietveld refinement (Cu–$K_{\alpha 1}$; $\lambda = 1.5406$ Å).

The three-dimensional framework of this phosphate can be considered as composed of an alternation of BaO_{10} polyhedra, PO_4 tetrahedra, and $Sb(Fe)O_6$ octahedra. The BaO_{10} polyhedra and $Sb(Fe)O_6$ octahedra share edges and form infinite chains parallel to the c-axis. Each $Sb(Fe)O_6$ octahedron is connected at its vertices to six PO_4 tetrahedral groups. The PO_4 tetrahedra are isolated, and each is linked, through two of its edges, to two BaO_{10} polyhedra. The three-dimensional framework consists of layers of Ba^{2+} cations in tenfold coordination, alternating with dense layers made up of MO_4 octahedra (M = Sb, Fe) and PO_4 tetrahedra, which are interconnected via their vertices (Figures 2 and 3).

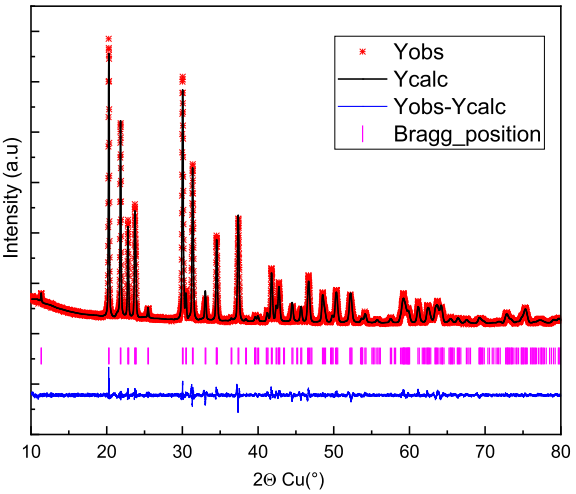

Figure 1. Rietveld refinement of the $BaSb_{0.5}Fe_{0.5}(PO_4)_2$ phase.

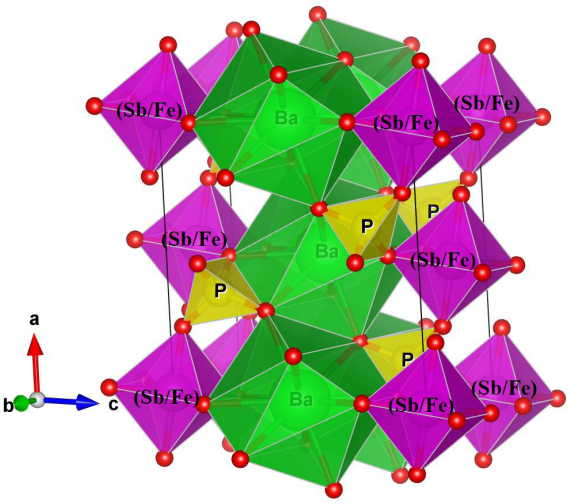

Figure 2. Structure of the $BaSb_{0.5}Fe_{0.5}(PO_4)_2$ phase.

3.2. *Scanning electron microscopy (SEM)*

SEM Investigation by SEM of the $BaSb_{0.5}Fe_{0.5}(PO_4)_2$ powder (Figure 4), recorded at 2000× and 3000× magnifications, revealed a heterogeneous microstructure consisting of agglomerated grains of various sizes, interspersed with intergranular pores. The grains exhibit irregular morphology and clustering behavior, indicative of polycrystalline growth

Table 1. Crystallographic data for $BaSb_{0.5}Fe_{0.5}(PO_4)_2$

Space group $C2/m$ (N° 12); [$Z = 2$; $a = 8.1661$ (4) Å; $b = 5.1934$ (3) Å; $c = 7.8212$ (4) Å; $\beta = 94.51$ (1)°; $V = 331$ (1) Å^3]						
Experimental data						
Temperature 25 °C; angular range $10° \leq 2\theta \leq 80°$						
step scan increment (2θ): 0.0105°						
Zero point (2θ), −0.021 (1)°						
Profile parameters						
Pseudo-Voigt function, PV = ηL + (1 − η)G; $\eta = 0.586$ (2)						
Half-width parameters, $U = 0.369$ (3), $V = -0.0597$ (4), and $W = 0.0120$ (1)						
Conventional Rietveld R-factors, $R_{WP} = 6.7\%$; $R_P = 4.9\%$; $R_B = 2.20\%$; $R_F = 1.59\%$						
Atom	Site	Wyckoff positions			B_{iso} (Å^2)	Occupancy
Ba	2c	0	0	0.5	0.7 (1)	1
(Fe/Sb)	2a	0	0	0	0.3 (2)	0.5/0.5
P	4i	0.3644 (1)	0	0.2045 (1)	0.4 (1)	1
O (1)	4i	0.2342 (3)	0	0.0560 (2)	0.7 (4)	1
O (2)	4i	0.3106 (2)	0	0.3854 (2)	0.4 (3)	1
O (3)	8j	0.4839 (3)	0.2414 (2)	0.1922 (1)	0.6 (2)	1

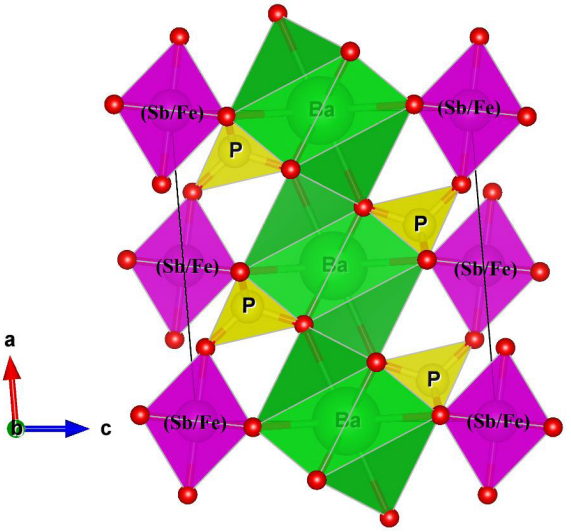

Figure 3. Projection onto the (ac) plane of the structure of the $BaSb_{0.5}Fe_{0.5}(PO_4)_2$ phosphate.

with incomplete densification, a common feature in materials synthesized at moderate temperatures. Based on the scale bars (30 µm and 20 µm), the individual grains and clusters display approximate sizes ranging from 2 to 10 µm, with some larger agglomerates extending beyond 10 µm. Such a morphology could influence the material's functional properties, particularly in relation to surface activity and ionic diffusion paths.

To evaluate the elemental composition of the synthesized material and verify the target stoichiometry, energy-dispersive X-ray spectroscopy (EDS) was performed. The quantitative results obtained from the EDS spectra (Figure 5 and Table 3) provide the mass and atomic percentages of the elements Ba, Fe, Sb, P, and O in the compound studied. From the atomic percentages, the calculated ratios (Ba/P = 0.557, Fe/P = 0.284, Sb/P = 0.307, Ba/Sb = 1.82, and Ba/Fe = 1.96) align well with the theoretical values for the $BaSb_{0.5}Fe_{0.5}(PO_4)_2$ composition (Ba/P = 0.50, Fe/P = 0.25, Sb/P = 0.25, Ba/Sb = 2.00, and Ba/Fe = 2.00). The small deviations observed are typical of EDS quantification due to matrix effects and the limited sensitivity for light elements. Nevertheless, the overall consistency between experimental and theoretical ratios confirms that the targeted stoichiometry is achieved, indicating successful incorporation of Sb and Fe in the structure. This result strongly supports the homogeneity of the sample, and the effectiveness of the synthesis route used for producing a well-defined, single-phase phosphate compound.

Table 2. Powder diffraction data of $BaSb_{0.5}Fe_{0.5}(PO_4)_2$ (Cu–$K_{\alpha 1}$; λ = 1.5406 Å)

hkl	d_{obs} (Å)	100 I/I_0 (obsd)	100 I/I_0 (calcd)	hkl	d_{obs} (Å)	100 I/I_0 (obsd)	100 I/I_0 (calcd)
001	7.7970	5	5	132	1.5449	6	5
110	4.3783	100	100	−422	1.5150	6	5
200	4.0704	64	68	−224	1.4887	5	4
002	3.8985	34	32	−512	1.4811	3	3
−111	3.8884	15	16	314	1.4654	4	5
111	3.7506	39	39	−404	1.4667	4	4
−201	3.7306	22	21	330	1.4602	7	6
201	3.4944	3	4	422	1.4502	5	6
−112	2.9747	92	90	224	1.4271	2	1
−202	2.9330	10	10	512	1.4063	2	3
112	2.8523	52	53	−332	1.3871	1	1
202	2.7111	9	10	600	1.3552	2	2
020	2.5990	31	29	332	1.3489	1	1
310	2.4051	34	36	040	1.3000	3	3
−311	2.3447	1	1	−134	1.2902	2	2
−203	2.2776	3	2	134	1.2693	2	2
311	2.2544	2	2	−116	1.2619	5	4
220	2.1945	5	4	240	1.2372	1	1
022	2.1612	18	17	042	1.2323	1	1
−221	2.1312	7	6	206	1.2108	2	1
−312	2.1137	14	12	424	1.2016	3	3
400	2.0352	5	6				
312	1.9860	6	6				
004	1.9493	16	14				
222	1.8753	9	9				
−402	1.8653	4	4				
−313	1.8299	3	3				
−204	1.8159	9	9				
−114	1.8144	11	10				
114	1.7534	7	7				
402	1.7479	6	9				
130	1.6933	4	3				
131	1.6491	2	2				
420	1.6018	3	4				
−132	1.5625	10	9				
510	1.5536	5	5				

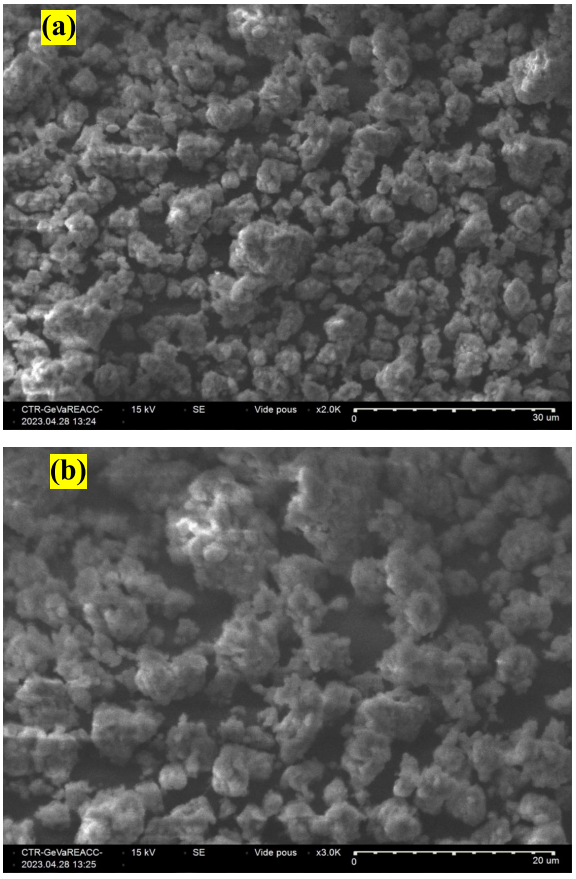

Figure 4. SEM micrographs of $BaSb_{0.5}Fe_{0.5}(PO_4)_2$ at 2000× (a) and 3000× (b) magnifications.

Table 3. EDX composition analysis of $BaSb_{0.5}Fe_{0.5}(PO_4)_2$

Element	Weight (%)	Atom (%)
C	15.0	32.0
O	30.6	49.2
P	10.6	8.8
Fe	5.2	2.5
Sb	12.6	2.7
Ba	26.0	4.9
Total	100.0	100.0

3.3. *Infrared and Raman study*

Raman and infrared spectroscopic analyses were carried out to obtain a deeper understanding of the bonding environment within the $BaSb_{0.5}Fe_{0.5}(PO_4)_2$ compound. Given that its structure consists of both isolated PO_4 tetrahedra and $Sb(Fe)O_6$ octahedra, its vibrational features are characteristic of orthophosphates. The vibrational behavior of PO_4 tetrahedral units is well established, and in such structures, the vibrational modes of the phosphate groups typically dominate over lattice vibrations and metal–oxygen interactions. Raman and IR spectra of the $BaSb_{0.5}Fe_{0.5}(PO_4)_2$ phase are given in Figures 6 and 7. The vibrational behavior of the phosphate units in the $BaSb_{0.5}Fe_{0.5}(PO_4)_2$ compound was investigated through infrared and Raman spectroscopic techniques. The analysis revealed distinct vibrational bands corresponding to the internal modes of the PO_4^{3-} tetrahedra, consistent with expectations for well-ordered phosphate frameworks.

The symmetric non-degenerate stretching mode (ν_1) of the P–O bond was clearly observed in the 918–1023 cm^{-1} spectral range, which is typical for isolated tetrahedral phosphate groups. This band is usually the most intense in infrared spectra and serves as a strong indicator of the presence of PO_4 units.

In the low-frequency region between 429 and 485 cm^{-1}, vibrational features were identified that correspond to the antisymmetric doubly degenerate bending modes (ν_2) of the PO_4 tetrahedra. These modes are sensitive to distortions within the tetrahedron and can reflect subtle differences in the local structural environment around the phosphate group.

The high-frequency region ranging from 1050 to 1157 cm^{-1} exhibited bands attributed to the triply degenerate O–P–O asymmetric stretching modes (ν_3). The presence of these modes further confirms the integrity of the phosphate framework and the preservation of tetrahedral symmetry, albeit slightly distorted due to cation substitution.

Additionally, the bands detected in the 526–657 cm^{-1} region were assigned to the harmonic bending vibrations of O–P–O linkages (ν_4). These bending modes are characteristic of internal deformations within the PO_4 group and are commonly used to evaluate the degree of distortion in the tetrahedral geometry.

Altogether, the vibrational spectra confirm the presence and stability of the phosphate units within the crystal structure and support the assignment of $BaSb_{0.5}Fe_{0.5}(PO_4)_2$ to the yavapaiite-type framework, where the PO_4 groups retain a nearly ideal tetrahedral configuration, as commonly observed in yavapaiite phosphates [12–18].

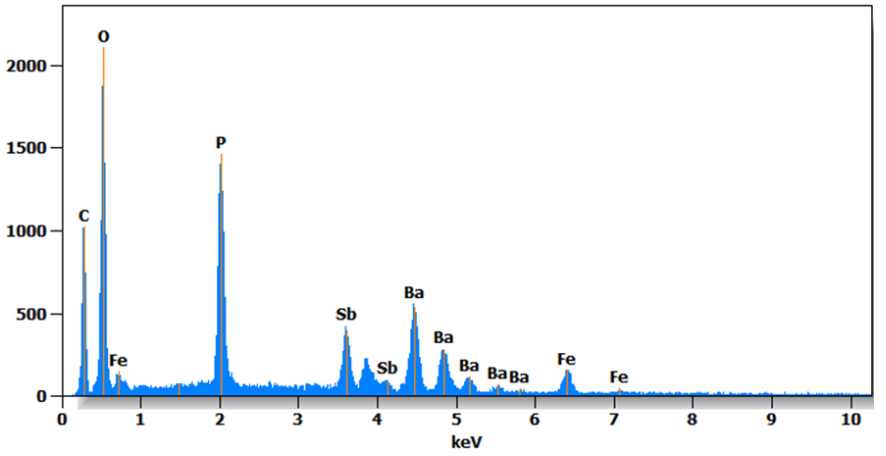

Figure 5. EDX spectrum of $BaSb_{0.5}Fe_{0.5}(PO_4)_2$.

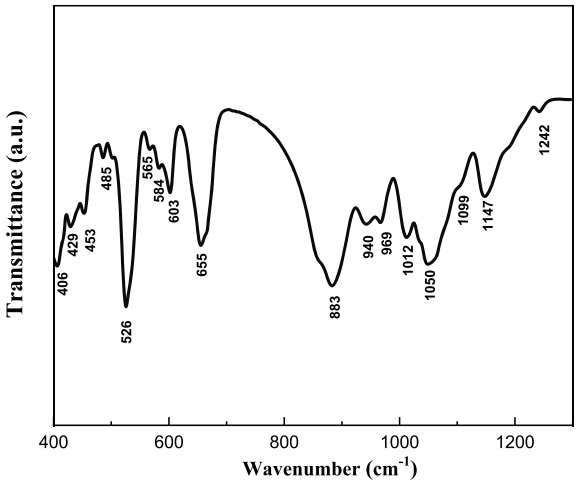

Figure 6. Infrared spectrum of $BaSb_{0.5}Fe_{0.5}(PO_4)_2$.

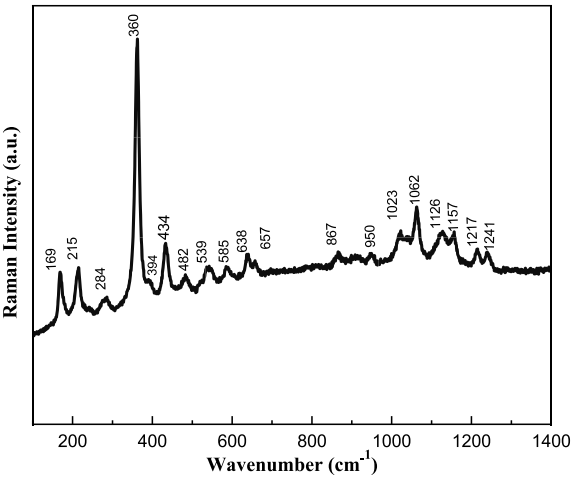

Figure 7. Raman spectrum of $BaSb_{0.5}Fe_{0.5}(PO_4)_2$.

In the lattice-mode region of Raman spectra (400–50 cm^{-1}), the translational modes of PO_4^{3-} ions as well as vibrational modes of PO_4^{3-} ions and BaO_{10} groups should be expected. At wavenumbers below 400 cm^{-1}, coupling occurs between the different bending vibrations O–P–O, O–Ba–O, Ba–O–P. The strong Raman bands observed at 360 cm^{-1} may be assigned to Fe–O stretching vibration modes [20]. The low-frequency modes observed below 284 cm^{-1} can be easily attributed to translational modes of the Ba^{2+}, Fe^{3+}, Sb^{5+}, and PO_4^{3-} ions.

3.4. *UV–visible analysis*

The optical properties of $BaSb_{0.5}Fe_{0.5}(PO_4)_2$ were studied at room temperature by measuring UV–visible absorption spectra (200–800 nm) shown in Figure 8. The UV–Vis absorption spectrum of the compound reveals a pronounced and broad absorption edge in the ultraviolet region (between 200 and 300 nm). This band is mainly attributed to ligand-to-metal charge transfer transitions, primarily $O^{2-} \rightarrow Fe^{3+}$, which is the main optically active center in the structure. A minor contribution from $O^{2-} \rightarrow Sb^{5+}$

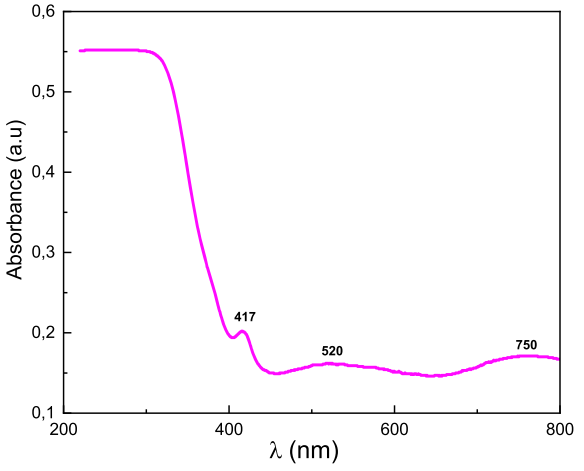

Figure 8. UV–visible absorption spectrum of $BaSb_{0.5}Fe_{0.5}(PO_4)_2$.

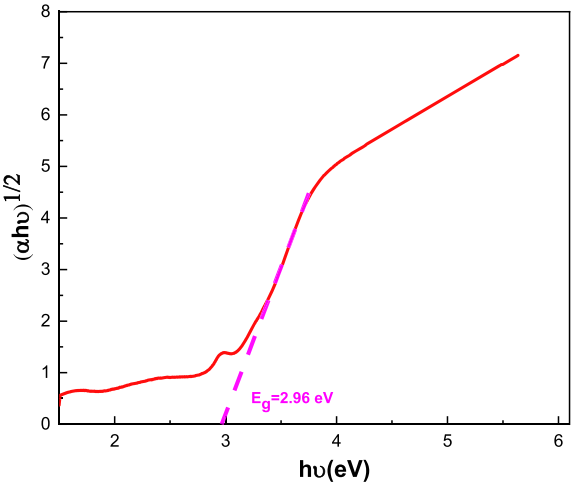

Figure 9. Plot of $(\alpha h\nu)^{1/2}$ versus $h\nu$ for $BaSb_{0.5}Fe_{0.5}(PO_4)_2$.

transitions cannot be excluded [14–17,21]. The optical spectrum of $BaSb_{0.5}Fe_{0.5}(PO_4)_2$ also shows three low-intensity bands centered around 750, 520, and 417 nm. According to the literature, these bands are attributed, respectively, to the forbidden transitions $^6A_{1g}$ (S) → $^4T_{2g}$ (G) (750 nm), $^6A_{1g}$ (S) → $^4T_{1g}$ (G) (520 nm), and $^6A_{1g}$ (S) → $^4A_{1g}$ (G), $^4E_{2g}$ (G) (417 nm) of the Fe^{3+} ions in octahedral sites [22].

The direct or optical indirect band gap energies E_g can be calculated for the salts using the Tauc equation (Equation (1)) [23]. The absorption coefficient α is determined using Equation (2) [24], where A and d indicate the absorbance and thickness of the cuvette used, respectively.

$$\alpha h\nu = B(h\nu - E_g)^m \quad (1)$$

$$\alpha = (2.3003A)/d \quad (2)$$

where h is the Planck constant, ν the photon frequency, B a constant, and m a constant determining the optical transition type.

Figures 9 and 10 show $(\alpha h\nu)^2$ and $(\alpha h\nu)^{1/2}$ variation versus $h\nu$ for $BaSb_{0.5}Fe_{0.5}(PO_4)_2$. The direct energy gap is estimated at E_g = 2.96 eV and indirect at E_g = 3.28 eV. As found elsewhere, band gaps estimated at 4.16 eV for $BaZr(PO_4)_2$ and 4.11 eV for $Ba_{0.97}Zr(PO_4)_2$:$0.03Eu^{3+}$ indicate a red shift in the optical band gap, which is attributed to the dopant Eu^{3+} ion generating intermediate energy levels around valence and conduction bands, leading to band gap narrowing [25]. Generally, the values obtained for

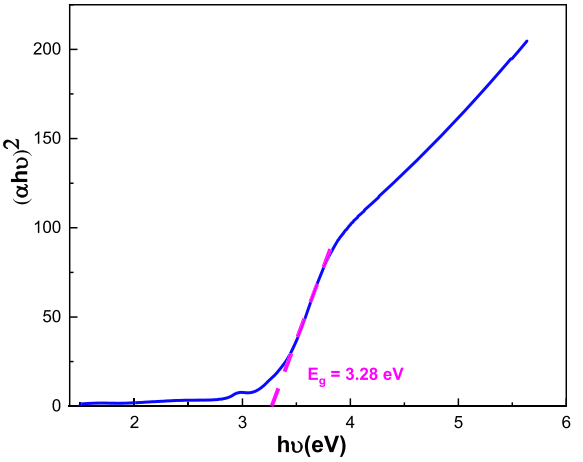

Figure 10. Plot of $(\alpha h\nu)^2$ versus $h\nu$ for $BaSb_{0.5}Fe_{0.5}(PO_4)_2$.

gap energies indicate a semiconductor character.

4. Conclusion

In this study, the phosphate-based compound $BaSb_{0.5}Fe_{0.5}(PO_4)_2$ was synthesized and structurally characterized. X-ray diffraction analysis confirmed that the compound crystallizes in the monoclinic yavapaiite-type structure, assigned to the $C2/m$ space group with Z = 2, consistent with structural trends observed in other $A^{II}M^{IV}(PO_4)_2$ systems where

the cationic size ratio plays a pivotal role in stabilizing ordered polyhedral frameworks.

The vibrational studies performed using infrared and Raman spectroscopy confirmed the presence of characteristic PO_4^{3-} vibrational modes. The spectral features agree with previously reported data for similar yavapaiite-type phosphates, indicating the retention of well-defined phosphate tetrahedra and supporting the structural assignment.

The optical absorption measurements revealed that $BaSb_{0.5}Fe_{0.5}(PO_4)_2$ exhibits a direct optical band gap of 2.96 eV and an indirect band gap of 3.28 eV, classifying it as a wide band-gap semiconducting material. These electronic characteristics suggest potential applications in optoelectronic devices, photocatalysis, or UV detection technologies.

Declaration of interests

The authors do not work for, advise, own shares in, or receive funds from any organization that could benefit from this article, and have declared no affiliations other than their research organizations.

References

[1] H. Y.-P. Hong, "Crystal structures and crystal chemistry in the system $Na_{1+x}Zr_2Si_xP_{3-x}O_{12}$", *Mater. Res. Bull.* **11** (1976), pp. 173–182.

[2] A. Aatiq, M. R. Tigha, R. Fakhreddine and A. Marchoud, "Structure and spectroscopic characterization of the two $PbSb_{0.5}Fe_{1.5}(PO_4)_3$ and $Pb_{0.5}SbFe(PO_4)_3$ phosphates with Nasicon type-structure", *J. Mat. Environ. Sci.* **6** (2015), pp. 3483–3490.

[3] A. Akhrouf, F. Lahnine, Y. Boudad, et al., "$Na_2Zn_{0.5}Co_{0.5}P_2O_7$ diphosphate: Sol-gel synthesis studies, and prospects as a novel supercapacitor electrode material", *Mater. Res. Bull.* **180** (2024), article no. 113020.

[4] Y. Ghandi, S. El Mazouzi, C. Moukhfi, H. Mabrak, A. Zourif, R. Fakhreddine, M. Tridane and S. Belaaouad, "Synthesis, structural characterization, and electrochemical properties of $MgNiP_2O_7$ for energy storage applications", *J. Eur. Phys. B* **98** (2025), no. 2, article no. 30.

[5] A. Aatiq, H. Bellefqih, A. Marchoud, R. Fakhreddine, N. Boudar and R. Tigha, "Structure of two new $K_2SnX(PO_4)_3$ (X = Cr, In) Langbeinite-type phases", *J. Mater. Environ. Sci.* **8** (2017), pp. 2940–2945.

[6] A. Akhrouf, Y. Laajali, M. Haddad, E. Hlil and S. Krimi, "Synthesis, structural, optical, thermal, magnetic and EPR investigations of the new phosphate $KCuCr(PO_4)_2$", *J. Mol. Struct.* **1258** (2022), article no. 132640.

[7] A. Leclaire, M. M. Borel, J. Chardon and B. Raveau, "A Mo(IV) monophosphate, $BaMo(PO_4)_2$, with the yavapaiite layer structure", *J. Solid State Chem.* **116** (1995), pp. 364–368.

[8] K. Popa, G. Wallez, D. Bregiroux and P. Loiseau, "$M^{II}Ge(PO_4)_2$ (M = Ca, Sr, Ba): Crystal structure, phase transitions, and thermal expansion", *J. Solid State Chem.* **184** (2011), pp. 2629–2634.

[9] K. Fukuda, A. Moriyama and T. Iwata, "Crystal structure, phase transition and anisotropic thermal expansion of barium zirconium diorthophosphate, $BaZr(PO_4)_2$", *J. Solid State Chem.* **178** (2005), no. 6, pp. 2144–2151.

[10] D. Bregiroux, K. Popa and G. Wallez, "Crystal chemistry of $M^{II}M^{IV}(PO_4)_2$ double monophosphates", *J. Solid State Chem.* **230** (2015), pp. 26–33.

[11] A. Aatiq, M. R. Tigha, R. Fakhreddine, D. Bregiroux and G. Wallez, "Structure, Infrared and Raman spectroscopic studies of newly synthesized $A^{II}(Sb^{V}_{0.5}Fe^{III}_{0.5})(PO_4)_2$ (A: Ba, Sr, Pb) phosphates with yavapaiite structure", *J. Solid State Sci.* **58** (2016), pp. 44–54.

[12] R. Fakhreddine and A. Aatiq, "Structure, Infrared and Raman spectroscopic studies of the new $Ba(Nb^{V}_{0.5}M^{III}_{0.5})(PO_4)_2$ (M^{III} = Al, Cr, Fe, In) yavapaiite compounds series", *J. Mediterranean Chem.* **8** (2019), no. 5, pp. 397–408.

[13] H. Bellefqih, R. Fakhreddine, A. Aatiq and M. R. Tigha, "Structure, infrared and Raman spectroscopic studies of new $A^{II}(Sb^{V}_{0.5}Cr^{III}_{0.5})(PO_4)_2$ (A = Ba, Sr, Pb) yavapaiite phases", *J. Mediterranean Chem.* **10** (2020), no. 8, pp. 734–743.

[14] R. Fakhreddine, A. Ouasri and A. Aatiq, "Synthesis, structural, morphology, spectroscopic and optical study of new metal orthophosphate $M^{II}(Sb_{0.5}Ga_{0.5})(PO_4)_2$ (M^{II} = Sr, Pb, Ba) compounds", *J. Solid State Chem.* **329** (2024), article no. 124439.

[15] R. Fakhreddine, M. R. Tigha, A. Ouasri and A. Aatiq, "Structural, morphological, Infrared-Raman, and UV studies of three yavapaiite phosphates $Ba(Sb^{V}_{0.5}M^{III}_{0.5})(PO_4)_2$ (M: Sc, In, Yb)", *J. Polyhedron* **267** (2025), article no. 117358.

[16] F. Rachid, M. R. Tigha, A.-I. Chham, N. Sajai, H. Bellefqih, A. Ouasri and A. Aatiq, "Synthesis, and crystal structure of phosphates with yavapaiite type-structure", in *Advanced Materials for Sustainable Energy and Engineering, ICAMSEE* (E. M. Elkhattabi, M. Boutahir, K. Termentzidis, K. Nakamura and A. Rahmani, eds.), Springer Proceedings in Energy, Springer: Cham, 2023.

[17] H. Bellefqih, E. Bilal, R. Fakhreddine, B. Mehdaoui, N. Haneklaus and A. Aatiq, "Structural, vibrational, and optical studies of newly synthesized Yavapaiite-type phases $BaSb_{2/3}X_{1/3}(PO_4)_2$ (X = Mn, Co, Cu, Zn)", *Inorg. Chem. Commun.* **163** (2024), article no. 112347.

[18] Y. Ghandi, R. Fakhreddine, C. Moukhfi, et al., "Innovative structural and optical insights into synthesized $BaTi_{(1-2x)}Sb_xCr_x(PO_4)_2$ ($0 \le x \le 0.5$) yavapaiite phases", *J. Solid State Chem.* **347** (2025), article no. 125305.

[19] J. Rodriguez-Carvajal, "FULLPROF: a program for Rietveld refinement and pattern matching analysis", in *Satellite meeting on powder diffraction of the XV congress of the IUCr, Toulouse*, vol. 127, 1990.

[20] F. Z. Tabane, R. Fakhreddine, F. Hamouche, et al., "Microstructural, spectroscopic and optical studies of the monophosphates $Ba(M_{0.50}Nb_{0.50})(PO_4)_2$ with M = Fe and In", *Mor. J. Chem.* **13** (2025), pp. 1643–1656.

[21] S. K. Skalli, R. Fakhreddine, B. Mehdaoui, A. Chakir, L. Bih, A. Aatiq and A. El Bouari, "Structural study and dielectric properties of high electrical resistance orthophosphate $Pb(Sb_{0.5}Al_{0.5})(PO_4)_2$: Combination of complex permittivity, impedance, AC conductivity, and modulus", *J. Electron. Mater.* **55** (2026), pp. 372–391.

[22] A. El Bouari, A. El Jazouli, S. Benmokhtar, P. Gravereaub and A. Wattiaux, "Synthesis, structure, magnetic, optical and Mössbauer properties of $Na_2FeSn(PO_4)_3$", *J. Alloys Compd.* **503** (2010), pp. 480–484.

[23] J. Tauc, R. Grigorovici and A. Vancu, "Optical properties and electronic structure of amorphous germanium", *J. Phys. State Solid (b)* **15** (1966), pp. 627–637.

[24] D. Doughri, B. Mehdaoui, R. Fakhreddine, A. El Bouari and J. Materials, "Structural, dielectric and ac ionic conductivity of Li_4FeSbO_6 oxide", *Chem. Phys.* **318** (2024), article no. 129310.

[25] S. Yadav, A. S. Rao and D. Meena, "Optical characteristics, Judd-Ofelt analysis of enhanced luminescence by flux in thermally stable, novel Eu^{3+} - doped $BaZr(PO_4)_2$ phosphor for indoor lighting applications", *J. Phys. B: Condens. Matter* **695** (2024), article no. 416522.